Eur. Phys. J. Appl. Phys. **97**, 49 (2022)

https://doi.org/10.1051/epjap/2022220138

THE EUROPEAN PHYSICAL JOURNAL APPLIED PHYSICS

Regular Article

Structural, dielectric and optical properties of Ta_2O_5-Bi_2O_3-P_2O_5 phosphate glasses

Mohamed Laourayed[1], Yasmina Alaoui[1], Asmae Er-rafai[1], Mouad El Mouzahim[1], Mouloud El Moudane[1,*], Mohammed Abid[2], Mestapha Beraich[3], Abdellah Guenbour[1], and Abdelkbir Bellaouchou[1]

[1] Laboratory of Materials, Nanotechnology, and Environment, Faculty of Sciences, Mohammed V University in Rabat, P.O. Box 1014, Agdal-Rabat, Morocco
[2] CRMEF, Laboratory of Scientific Research and Educational Innovation, Rabat, Morocco
[3] Laboratory of Materials, Energy and Environment, Physics Department, Faculty of Sciences Semlalia, Cadi Ayyad University, Marrakech, Morocco

Received: 21 April 2022 / Received in final form: 21 May 2022 / Accepted: 31 May 2022

Abstract. Glasses with the formula $5Ta_2O_5$-xBi_2O_3-$(95\text{-}x)P_2O_5$ for $10 \leq x \leq 20$ mol% were prepared using the standard melt-quench method and identified using X-ray diffraction, Differential Scattering Calorimetry, and Infrared spectroscopy. Furthermore, the dielectric and optical characteristics were determined. The glass transition temperature (T_g) increases linearly with bismuth oxide content, from 524 °C for $x = 10$ mol% to 582 °C for $x = 20$ mol%. When the amount of Bi_2O_3 in the system increases, the density rises and the molar volume (V_M) decreases. The Infrared spectroscopy shows the presence of BiO_6 and PO_3 structural groups and reveals the depolymerization of the phosphate links by the creation of the Bi–O–P groups. Replacing P_2O_5 by Bi_2O_3 shows that the dielectric constant ε_r' and dielectric losses tanδ vary with the concentration of added Bi_2O_3. Optical characteristics of the investigated glasses were determined using UV–vis spectroscopy and the energy band gap has been estimated.

1 Introduction

The significance of glass is shown by its use in a number of areas like solid state batteries [1], solar cells [2], optical properties [3]. Among them, phosphate glasses are widely described, but are often hampered by their poor chemical durability. The addition of transition metal oxides to later glasses usually enhances chemical and thermal resistance and stability [4–7]. Many studies have indicated that modifications in the structure and physical characteristics of phosphate glasses are due to the incorporation of transition metal oxides like WO_3, MoO_3, V_2O_5, Nb_2O_5 or Ta_2O_5 [8–15]. Transition metal oxides employed as network intermediaries in the glass also tend to enhance the non-linear optical characteristics [16, 17], and increase the refractive index [18,19]. Similarly, the addition of Bi_2O_3 has attracted the attention of several researchers due to their different properties [20,21]. In this direction, El Moudane et al. [22,23] showed that the electrical conduction of glasses containing different concentrations of Bi_2O_3 and depends on the frequency and temperature [23]. Many authors have investigated the electrical characteristics of bismuth-based glass with a variety of transition metals [24-26]. Their conclusions indicated that conduction property in such glasses arises from the short polaron hop among the transition elements in the different valence forms of the metals. It has been seen that the dielectric values of these glasses are best interpreted by the dipole relaxation theory with a relaxation time distribution. Moreover, their strong values of the constant dielectric seen have generally assigned to the strong polarizability of Bi (III) ion on the relaxation dipoles that develop in the valence state of two metal ions [27,28].

In the present study, tantalum-bismuth phosphate glasses with the composition $5Ta_2O_5$-xBi_2O_3-$(95–x)$ P_2O_5 for $10 \leq x \leq 20$ mol% were synthesized and characterized by DSC and IR spectroscopy. In addition, other properties including density, molar volume, glass transition temperature, dielectric and optical properties are also studied, and the optical gap energy has been calculated. The effect of Bi_2O_3 composition on dielectric and optical measurements was explored.

2 Experimental

The glasses were made using Ta_2O_5, Bi_2O_3, and $NH_4H_2PO_4$ of the analytical quality. Ammonium dihydrogen phosphate is thermally decomposed to produce P_2O_5, NH_3 and H_2O. Glassy samples of composition $5Ta_2O_5$-xBi_2O_3-$(95\text{-}x)$ P_2O_5 with $10 \leq x \leq 20$ mol% were prepared according to the following reaction:

* e-mail: m.elmoudane@gmail.com

Table 1. Composition (mol%), density ρ (g cm^{-3}), molar volume V_M (cm^3 mol^{-1}) and glass transition temperature T_g (°C) of the studied specimens.

Glass code	Ta_2O_5	Bi_2O_3	P_2O_5	ρ	V_M	T_g
x_1	5	10	85	6.17 ± 0.03	69.07 ± 0.03	524 ± 5
x_2	5	12.5	82,5	6.29 ± 0.03	68.02 ± 0.03	542 ± 5
x_3	5	15	80	6.49 ± 0.03	65.91 ± 0.03	554 ± 5
x_4	5	20	75	6.68 ± 0.03	63.63 ± 0.03	582 ± 5

$$5Ta_2O_5 + xBi_2O_3 + (95 - x)P_2O_5 \rightarrow 5Ta_2O_5 - xBi_2O_3 - (95 - x)P_2O_5$$

The appropriate ground compounds were placed into an alumina pot and fired for 12 h in the range of 200 °C to 500 °C in which NH_3 and H_2O were evaporated. The operating temperature was gradually heated to 1100 °C and maintained at this level over 30-minute period. The melted glasses were subsequently soaked at ambient conditions in atmospheric environment to yield glassy specimens. The vitreous material was kept in glass tubes and preserved in desiccants to avoid possible humidity damage. Table 1 presents the sample chemical concentrations of the investigated materials. More details are already published in a previous work [29].

3 Analysis and characterization techniques

3.1 X-ray diffraction

Room temperature X-ray diffractograms were plotted with a Siemens D5000 diffractometer against CuK radiation ($\lambda = 1.5418$ Å) in the 2ϑ range of 10–60° at a scan speed of 2° per minute. The amorphous nature of the sample was all but assured by XRD analysis.

3.2 Density and molar volume measurements

The density was determined at room temperature by the Archimedean technique with diethyl phthalate as the immersion liquid. The estimated error of the measurements was around ± (0.03 g cm^{-3}).

3.3 DSC study

The evaluation of the temperature of glass transition on 20–30 mg of the samples by the means of the method of DSC–SETARAM type apparatus 121 with a heating rate of 10°C/min in an argon atmosphere, with a precision of ± 5 °C.

3.4 Infrared spectroscopy

FTIR-ATR determination of the materials was achieved on a Jasco 4600 FT/IR Spectrometer with the Jasco ATR PRO ONE module. The specimens were analyzed in transmission mode with a 4 cm^{-1} resolution in the 1400–400 cm^{-1} region.

3.5 Dielectric properties

Dielectric measurements were taken on samples in the form of two-sided parallel plates, polished and coated with a silver paste to make high quality electrodes. The capacity C value was measured by means of a Philips PM 6302 automatic bridge, at a frequency of 10 kHz, and at a range of temperatures from 100 to 600 °C. The constant dielectric ε'_r, has been computed with the use of the equation:

$$\varepsilon'_r = \frac{Cd}{\varepsilon_0 A}$$

where, is the permittivity of free space, C is the capacitance, d is the thickness of the glass sample, and A is the cross-sectional surface area of specimen. The dielectric loss tan was calculated using the following formula:

$$\tan\delta = \frac{1}{2\pi f \rho \varepsilon'_r \varepsilon_0}$$

with f is the applied field frequency and ρ the electrical resistivity.

3.6 Optical measurements

Optical absorption determinations were carried out by means of a JASCO V-670 spectrophotometer associated with a sphere integral. This device makes it possible to study absorption over a wide spectral range extending from 250 nm (ultraviolet) to 800 nm (visible). The sample is in the form of a polished glass a few millimeters thick.

4 Results and discussion

4.1 X-ray diffraction

The amorphous character of the material has been further enhanced by the absence of Bragg peaks in the X-ray diffractogram of the glasses $5Ta_2O_5$-xBi_2O_3-(95-x)P_2O_5 with $10 \leq x \leq 20$ mol% (Fig. 1), the observed glasses were not hygroscopic.

4.2 Thermal analysis

It is interesting to note that the glass transition temperature (T_g) is determined from the DSC curve by

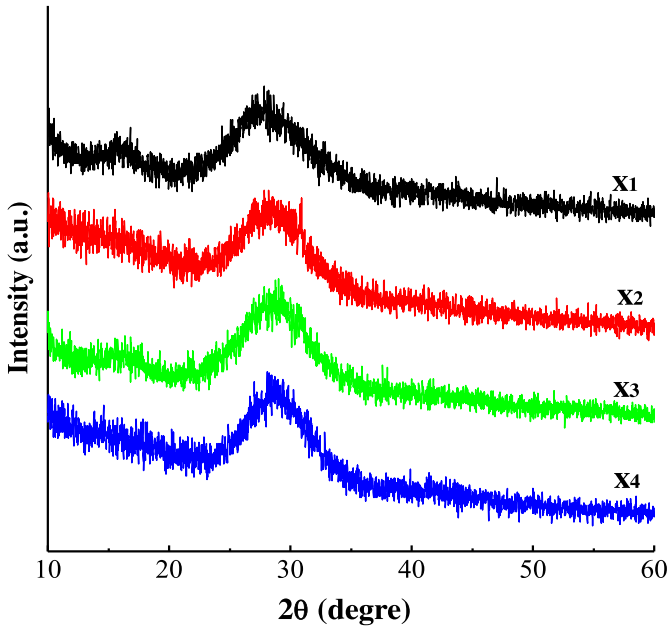

Fig. 1. XRD patterns of $5Ta_2O_5$-xBi_2O_3-(95-x)P_2O_5 glasses ($10 \leq x \leq 20$ mol %).

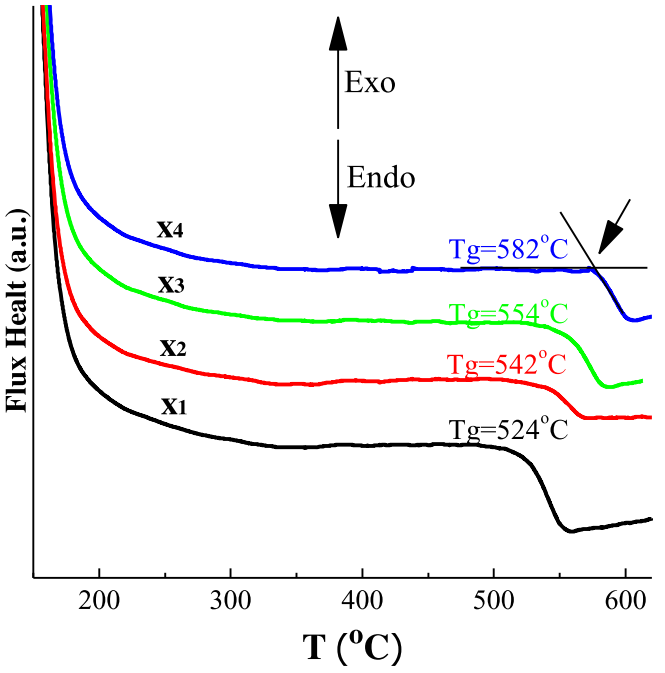

Fig. 2. DSC of glass for $5Ta_2O_5$-xBi_2O_3-(95-x)P_2O_5 ($10 \leq x \leq 20$ mol%).

considering the point of deviation from the baseline. An intersection point is added to DSC thermogram for the 10 mol% Bi_2O_3 content in Figure 2 to determine the T_g value.

The presence of the glass transition characteristic in the DSC thermograms of the samples further confirmed the glassy nature (Fig. 2). The DSC pattern of samples $5Ta_2O_5$–xBi_2O_3–(95–x)P_2O_5 with $10 \leq x \leq 20$ mol% indicates an endothermic peak that represents the glass transition (Fig. 2). The resulting values of the glass transition temperature show the variation of T_g from 524 °C for $x = x_1$ to 582 °C for $x = x_4$ with $\Delta T_g = 58$ °C (Tab. 1). Figure 3 illustrates that T_g linearly rises with increasing Bi_2O_3 content. The glass transition temperature is a measure of the thermal stability of the structural network. Therefore, the rise in T_g suggests that the network structure is growing stronger, due to the replacement of the P_2O_5 by Bi_2O_3 in $5Ta_2O_5$-xBi_2O_3-(95-x)P_2O_5 phosphate glasses and could be related to the increase in the compactness of the glass structure, which is in good agreement with the increase in density. It also indicates that bismuth promotes the formation of strengthened bonds. Indeed, the addition of Bi_2O_3 increases the stability in the glass matrix through the formation of more stable P-O-Bi bonds.

4.3 Density and molar volume

Table 1 shows the values of ρ and V_M, which are plotted as a function of Bi_2O_3 concentration in Figure 4.

It is shown that the density ρ increases linearly with the substitution of P_2O_5 by Bi_2O_3. The molecular weight (M_W = 465.96 g mol^{-1}) of Bi_2O_3 is much higher compared with P_2O_5 (M_W = 141.94 g mol^{-1}), giving the rise in the density. On the other side, the molar volume diminishes linearly with increasing Bi_2O_3 concentration. This can be explained by the fact that the formation of Bi–O is at the expense of the P–O bands, which function to cross-link the phosphate network, and lead to the closing of the network structure. The vacuum of several oxygen anions work in reducing the molar volume [30,31].

4.4 Spectral Infrared study

To identify the main characteristics of the local glass structure, absorption FT–IR measurements are performed. The infrared spectra at ambient temperature in the range 400–1400 cm^{-1} of the specimens are presented in Figure 5.

We observe the symmetrical stretching vibration band ν_s (PO_2) at 1150 cm^{-1} [32,33], which is characteristic of phosphate glasses. The band seen at 1075 cm^{-1} corresponds to the ν_{as} (PO_3) groups (chain terminator) [34], as do the λ_s of the PO_3 groups (chain terminator groups) at 970 and 1040 cm^{-1} [35], the ν_{as} POP groups possessing at 870 cm^{-1} [36,37], and the ν_s POP at 735 cm^{-1} [38] and the bending vibration (δ) of the $(P–O)^-$ linkages [32,35,38] 545 and 485 cm^{-1}. In another respect, these glasses show two typical P–O–P bridge bands around 870 and 735 cm^{-1} for the asymmetric and symmetric modes, respectively; this confirms the presence of pyrophosphate groups [36].

On the other hand, all the frequencies observed below 380 cm^{-1} are allocated to the vibrational mode of the Bi–O and Bi–O–Bi bonds [39–30]. The simultaneous appearance of two bands attributed to the P–O–P bridge can be regarded as correct evidence for the presence of $(P_2O_7)^{2-}$ groups [32,41]. Therefore, in this investigation, the observation that Bi_2O_3 addition leads to the depolymerization of the P–O–P bonds by rupture of the structural links and insertion of the distorted octahedral BiO_6. These findings lead to the notion that Bi_2O_3 embedded in the glass matrix has a network nature as shown by the DSC.

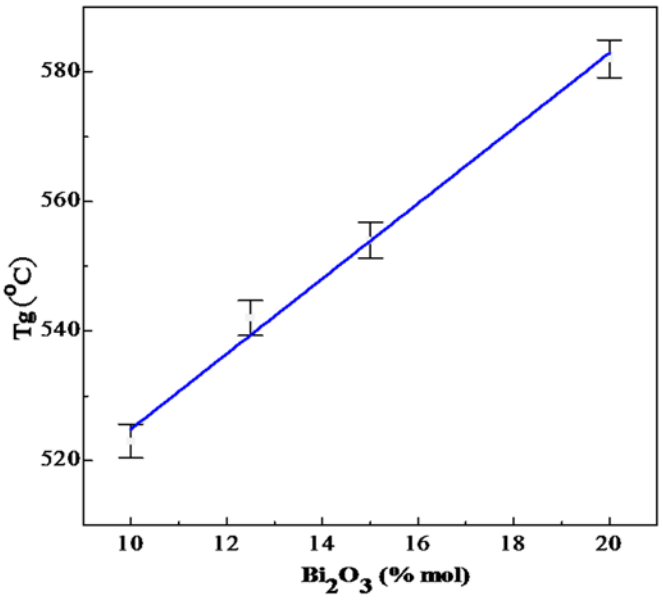

Fig. 3. Composition versus T_g for $5Ta_2O_5$-xBi_2O_3-$(95\text{-}x)P_2O_5$ with $10 \leq x \leq 20$ mol%.

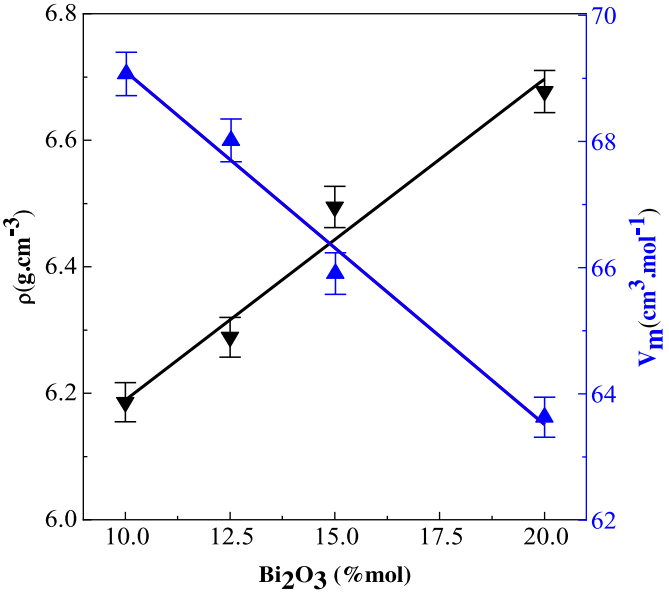

Fig. 4. Density and molar volume vs Bi_2O_3 content of $5Ta_2O_5$-xBi_2O_3-$(95\text{-}x)P_2O_5$ ($10 \leq x \leq 20$ mol %).

Hence, Bi^{3+} ions are incorporated into the lattice and create a P–O–Bi bond. Moreover, it can also be seen that the vibrations of the $\nu_{as}(PO_3)$ and $\nu_s(PO_3)$ corresponding to the end groups chains, are decreasing in intensity, this is allocated to the enrichment of the glass construction by non–bridging oxygen's (NBO) and cross-linking via the formation of P–O–Bi or P–O–Ta bonds.

4.5 Dielectric measurements

The permittivity (or dielectric constant) and the dielectric loss represent the polarizability of the material and the energy loss due to polarization and ionic conduction, respectively. The increase in these dielectric constants at low frequencies is due to the fact that charge carriers and defects at low frequencies can easily diffuse from one site to another, and the applied electric field favors charge carrier hopping between sites. Their accumulation at high barrier sites leads to an increase in polarization [42].

Figure 6 shows the variation of ε_r' with temperature for different Bi_2O_3 concentrations at 10 kHz. It can be seen that ε_r' shows an enhancement at higher temperatures. Similar shape is observed in Figure 7 for the variation of the dielectric loss tan with temperature at 10 kHz. There are distinct maxima in these plots, with the concentration of Bi_2O_3 rising. The impact of Bi_2O_3 content on the relaxation strength of such glasses can be seen from Figure 7. As the temperature increases, bismuth oxide is found to affect the permittivity of the glasses. The addition of 10–20 mol% Bi_2O_3 increases the dielectric constant and reduces the dielectric losses. For example, at 350 °C, the dielectric constant of the studied glasses increases from 7.04 for x1 glass to 10.8 for x4 glass.

The opposite behavior was observed for the dielectric losses tanδ (Tab. 2). This can be explained by the fact that the frequency jump of the charge carriers approaches that of the applied field as the temperature increases above 350 °C [43]. We also note that the relaxation temperature region shifted to higher temperatures with decreasing values of $(\tan\delta_{max}$ as the Bi_2O_3 content rises.

The strong rise in the value of ε_r' and tanδ (above the relaxation zone) with the temperature at 10 kHz may be ascribed to the polarization of the space charge. Indeed, other contributions for dielectric constant like electronic and orientation polarization do not increase with temperature. The reason for this result can be summarized as follows: (i) an enhancement in the density of BiO_6 units, (ii) an enhance in the asymmetrical P–O–Bi bending vibrations, (iii) the bond defaults generated in the glass lattice that participate in the polarization of the space charge [44,45].

4.6 Optical measurements

Figure 8 shows the optical absorbance spectra of the trivalent Ta_2O_5–Bi_2O_3–P_2O_5 glasses in the visible and near UV range. We note a decrease in absorbance when the wavelength increases. On the opposite, it will rise as the Bi_2O_3 concentration increases.

The appearance of a peak in the vicinity of 360 nm is observed, the intensity of which increases with increasing Bi_2O_3 content with a small violet shift. According to Peng et al [46] the colour transformation of the sample from colourless to brown can be attributed to the thermal reduction of Bi^{3+}.The optical bands observed around 360 nm are probably attributed to transitions of Bi^0 particles according to:

$$O^{2-}(2p^6) + Bi^{3+}(6p^0) \rightarrow O^{-}(2p^5) + Bi^0(6p^3)$$

It should also be noted that crystalline and non-crystalline materials are characterized and described by the optical band gap energy parameter. The latter is due to transitions of electrons from the valence band to the

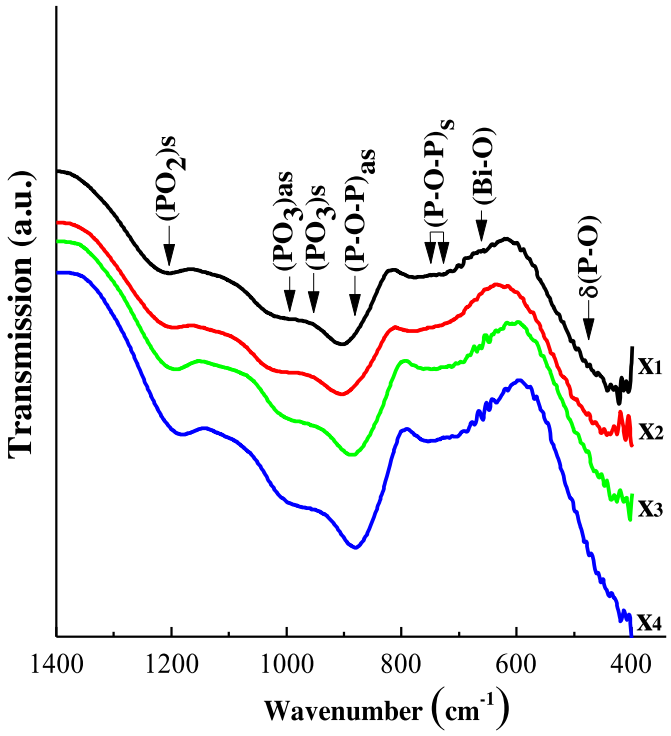

Fig. 5. IR spectra for $5Ta_2O_5$-xBi_2O_3-$(95\text{-}x)P_2O_5$ glasses ($10 \leq x \leq 20$ mol %).

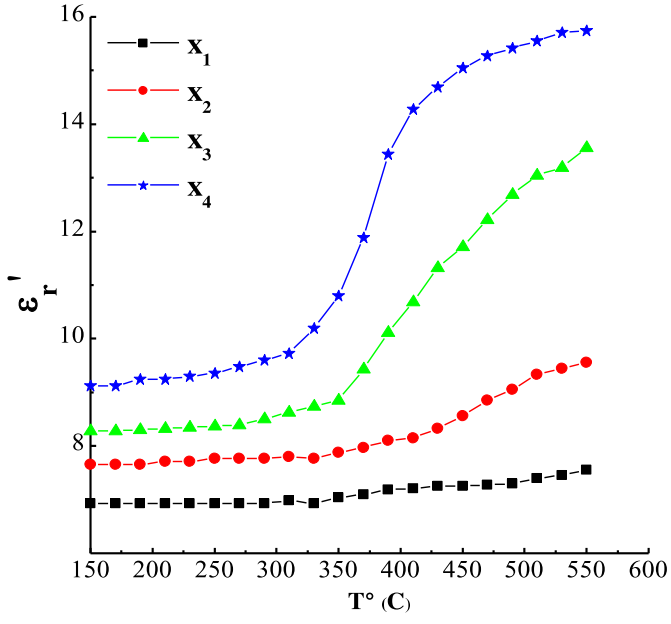

Fig. 6. versus temperature for $5Ta_2O_5$-xBi_2O_3-$(95\text{-}x)P_2O_5$ glasses ($10 \leq x \leq 20$ mol %) at 10 kHz.

conduction band through the band gap by interactions and absorption of electromagnetic waves. In this context, Davis and Mott used their theories [47] to estimate the optical band gap energy of amorphous materials by direct and indirect allowed transitions.

The absorption coefficient was found from the following relationship:

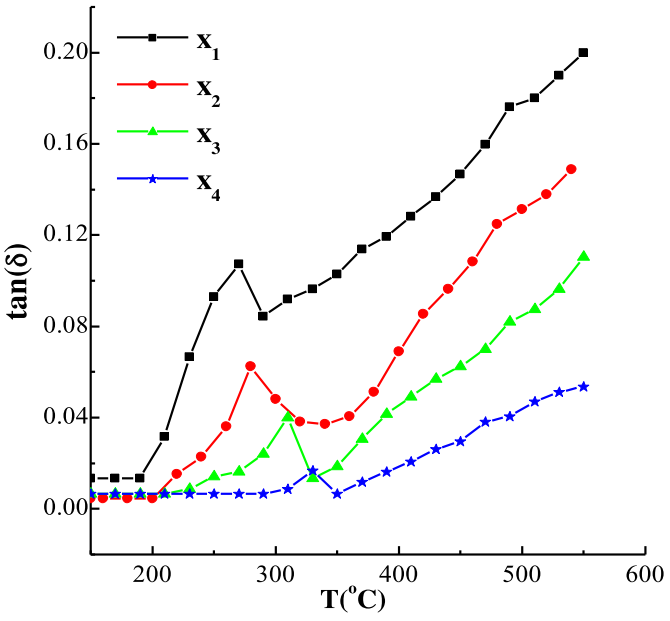

Fig. 7. Tanδ versus temperature for $5Ta_2O_5$-xBi_2O_3-$(95\text{-}x)P_2O_5$ glasses ($10 \leq x \leq 20$ mol %) at 10 kHz.

$$\alpha(\nu) = \frac{\ln\left(\frac{1}{T}\right)}{d} = 2.3\left(\frac{A}{d}\right)$$

d is the sample thickness, and A is the absorbance at the given frequency λ. The edge absorption for both direct and indirect band gaps is determined using the following formula:

$$\alpha(\nu) = \frac{B\left(h\nu - E_g\right)^p}{h\nu}$$

hν is the energy of the optical band gap, $h\nu$ is the energy of the photon, B is the band tail parameters, and p is the value of the number of indices which define the optical transition, that is to say $p = 1/2$ for the direct permitted transition, and $p = 2$ for the indirect permitted transition.

The direct and indirect permitted transition optical band gap was determined by extrapolating the zero-absorption linear region to be at $(\lambda)^{1/2} = 0$, and the values of the band tail parameter were also found from the slope of the curves. The Tauc plots for the $5Ta_2O_5$-xBi_2O_3-$(95\text{-}x)P_2O_5$ glasses are shown in Figure 9, and the E_g values are listed in Table 2. We observe that the E_g values reduce with increasing Bi_2O_3 content, passing from 3.55 eV to 4.80 eV (Fig. 9a) and from 4.00 eV to 5.20 eV (Fig. 9b) respectively for the direct and indirect permitted transitions. This decrease in E_g can be explained by the progressive increase in the population of non-bridging oxygens (NBO). In fact, the stimulation of the non-bridging oxygens (NBO) requires a lower energy than the bridging ones (BO), which generates a modification of the E_g [48,49]. The decrease in band gap energy with the introduction of Bi_2O_3

Table 2. Dielectric and band gap parameters of the studied glasses.

Glass code	ε'_r	tanδ	n	E_g (eV) Direct	Indirect
x_1	7.04	0.1	2.65	4.80 ± 0.06	5.20 ± 0.13
x_2	7.87	0.04	2.80	4.40 ± 0.08	4.84 ± ± 0.07
x_3	8.85	0.014	2.97	3.87 ± 0.11	4.31 ± 0.06
x_4	10.8	0.007	3.28	3.55 ± 0.05	4.00± 0.15

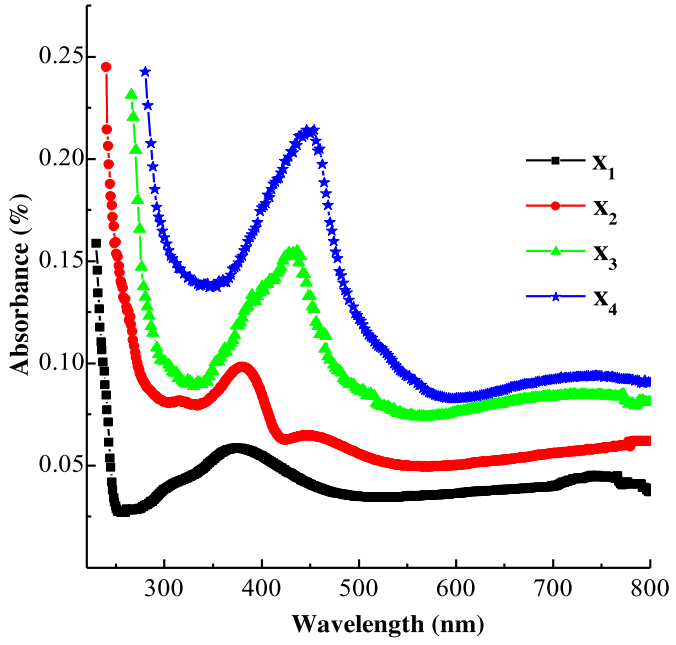

Fig. 8. The optical absorbance of $5Ta_2O_5$-xBi_2O_3-$(95\text{-}x)P_2O_5$ glasses ($10 \leq x \leq 20$ mol %).

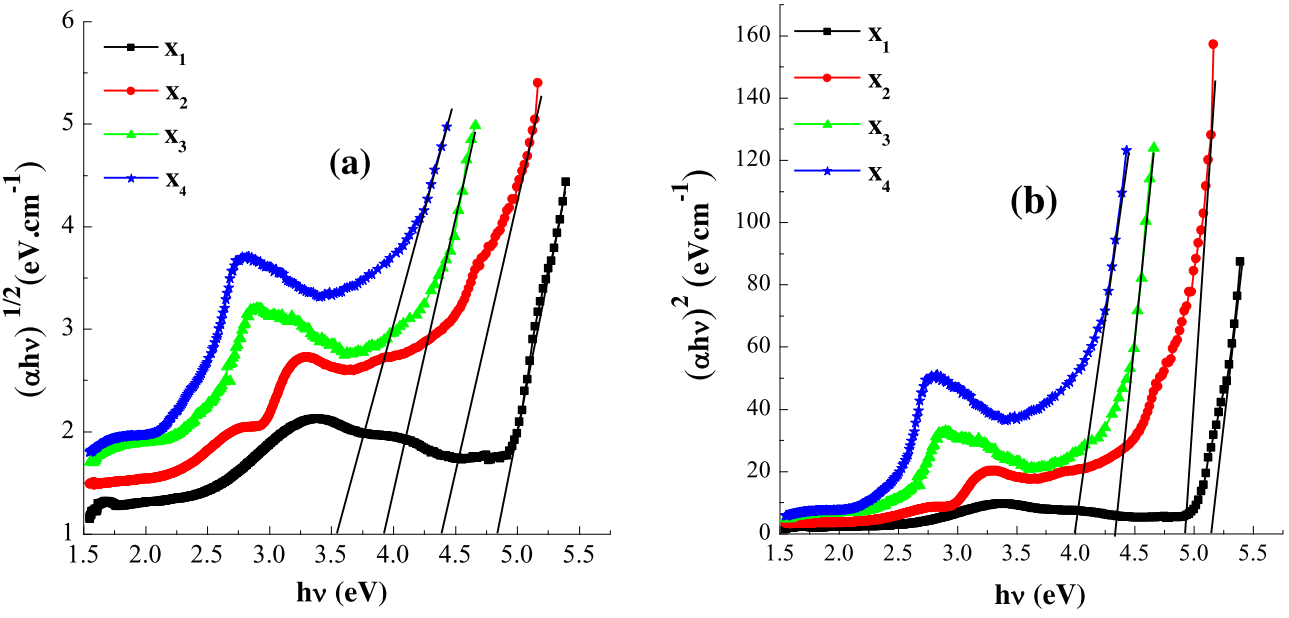

Fig. 9. Tauc's plots for $5Ta_2O_5$-xBi_2O_3-$(95\text{-}x)P_2O_5$ glasses ($10 \leq x \leq 20$ mol %): (a) direct ($p = 1/2$) and (b) indirect ($p = 2$).

can be attributed to the polarizing effect of Bi^{3+} ions and/or the increased overlap of the O(2p) oxygen orbitals and the 6s and 6p bismuth orbitals in the band gap. These results are in good agreement with the results published by Haily et al. [20], and by Rao et al. [50].

In order to correlate optical and electrical characteristics, we calculated the refractive index using the following relationship:

$$n = \sqrt{\varepsilon'_r}$$

where ε'_r is the relative dielectric permittivity.

The increase of the refractive index as a function of composition (Tab. 2), can be explained by the increase of the density in these glasses. This result is in good agreement with those obtained by DSC and IR spectroscopy.

Similarly, it has been reported that the refractive index (n) is shown to be dependent on the polarizability of the ions [51,52]. The ions that exhibit high polarizability in glasses are the oxygen ions that can have ionic, covalent or metallic bonds [52]. The polarizability of the bonds between the oxygen and the cations influences the refractive index. In our case, we have the formation of polarized bonds $P\text{-}O^{\delta-}...Bi^{\delta+}$, which increases the refractive index of these glasses.

5 Conclusion

In the present work, the glasses with composition $5Ta_2O_5$-xBi_2O_3-$(95–x)P_2O_5$ with $10 \leq x \leq 20$ mol% have been synthesized and some physical and chemical properties have been studied. To understand the structural evolution of these glasses, dielectric, optical, thermal, and spectroscopic properties have been combined. The increasing in the density, glass temperature transition, and the decreasing in the molar volume reveals that the presence of Bi_2O_3 in the glass matrix strengthens the structure of the glass. The changes in the dielectric and optical parameters by adding bismuth oxide are due to depolymerization of the glass network and an increase in the P-O-Bi bond's strength. When glasses are enriched by bismuth oxide, the polarizing effect of Bi^{3+} ions generates a decrease in the optical band gap.

Author contribution statement

This experimental study is part of the PhD thesis of M. Laourayed supervised by M. El Moudane who extensively participate to the writing of the manuscript. The synthesis, the characterization experiments, the data analysis and interpretation of the results were performed thanks to the participation of the authors Mohamed Laourayed, Yasmina Alaoui, Asmae Er-rafai, Mouad El Mouzahim, and Mouloud El Moudane. Thanks to the authors Mouloud El Moudane, Mohammed Abid, Mestapha Beraich, Abdellah Guenbour and Abdelkbir Bellaouchou who interpreted the optical properties and reviewed the manuscript. The authors declare no competing financial interests.

References

1. Y. Omori, T. Honma, T. Komatsu, J. Ceram. Soc. Jpn. **126**, 820 (2018)
2. B.L. Yu, A.B. Bykov, T. Qiu, P.P. Ho, R.R. Alfano, N. Borrelli, Opt. Commun. **215**, 407 (2003)
3. C. Devaraja, G.V.J. Gowda, B. Eraiah, K. Keshavamurthy, Ceram. Int. **47**, 7602 (2021)
4. M. Laourayed, M. El Moudane, M. Khachani, M. Boudalia, A. Guenbour, A. Bellaouchou, M. Tabyaoui, Mater. Today Proc. **13**, 974 (2019)
5. N.J. Kreidl, W.A. Weyl, J. Am. Ceram. Soc. **24**, 372 (1941)
6. A.S. Al-Hawery, J. Phys. Chem. Solids **58**, 1325 (1997)
7. J.J. Rothermel, K.-H. Sun, A. Silverman, J. Am. Ceram. Soc. **32**, 153 (1949)
8. M. Laourayed, M. El Moudane, A. Guenbour, M. Tabyaoui, A. Bellaouchou, A. Ghanimi, A. Sabbar, J. Mater. Environ. Sci. **8**, 2932 (2017)
9. G. Poirier, M. Poulain, Y. Messaddeq, S. Ribeiro, J. Non-Cryst. Solids **351**, 293 (2005)
10. G. Poirier, M. Nalin, L. Cescato, Y. Messaddeq, S.J.L. Ribeiro, J. Chem. Phys. **125**, 161101 (2006)
11. G. Poirier, F.S. Ottoboni, F.C. Cassanjes, Á. Remonte, Y. Messaddeq, S.J.L. Ribeiro, J. Phys. Chem. B **112**, 4481 (2008)
12. S.H. Santagneli, C.C. de Araujo, W. Strojek, H. Eckert, G. Poirier, S.J.L. Ribeiro, Y. Messaddeq, J. Phys. Chem. B **111**, 10109 (2007)
13. R. Stefan, D. Simedru, A. Popa, I. Ardelean, J. Mater. Sci. **47**, 3746 (2012)
14. C.L.J. De Lima, B. Pastena, R.P.R.D. Nardi, J.T.G. Junior, J.L. Ferrari, F.C. Cassanjes, G. Poirier, Mater. Res. **18**, 13 (2015)
15. L. Cordeiro, R.M. Silva, G.M. de Pietro, C. Pereira, E.A. Ferreira, S.J.L. Ribeiro, Y. Messaddeq, F.C. Cassanjes, G. Poirier, J. Non- Cryst. Solids **402**, 44 (2014)
16. E.L. Falcão-Filho, C.B. De Araújo, C.A.C. Bosco, L.H. Acioli, G. Poirier, Y. Messaddeq, G. Boudebs, M. Poulain, J. Appl. Phys. **96**, 2525 (2004)
17. D. Manzani, T. Gualberto, J.M.P. Almeida, M. Montesso, C. R. Mendonça, V.A.G. Rivera, L. De Boni, M. Nalin, S.J.L. Ribeiro, J. Non- Cryst. Solids **443**, 82 (2016)
18. N. Nowak, T. Cardinal, F. Adamietz, M. Dussauze, V. Rodriguez, L. Durivault-Reymond, C. Deneuvilliers, J.-E. Poirier, Mater. Res. Bull. **48**, 1376 (2013)
19. R.R. Gonçalves, J.J. Guimarães, J.L. Ferrari, L.J.Q. Maia, S. J.L. Ribeiro, J. Non- Cryst. Solids **354**, 4846 (2008)
20. E. Haily, L. Bih, A. El Bouari, A. Lahmar, M. El Marssi, B. Manoun, Phase Transitions **93**, 1030 (2020)
21. E. Haily, L. Bih, A. El bouari, A. Lahmar, M. Elmarssi, B. Manoun, Mater. Chem. Phys. **241**, 122434 (2020)
22. M. Elmoudane, M. Et-tabirou, M. Hafid, Mater. Res. Bull. **35**, 279 (2000)
23. M. El Moudane, M. El Maniani, A. Sabbar, A. Ghanimi, M. Tabyaoui, A. Bellaouchou, A. Guenbour, Mater. Res. Bull. **72**, 241 (2015)
24. S. Hazra and A. Ghosh, J. Phys.: Condens. Matter **9**, 3981 (1997)
25. A. Ghosh, J. Appl. Phys. **65**, 227 (1989)
26. A. Ghosh, J. Appl. Phys. **66**, 2425 (1989)
27. M. Laourayed, M. Moudane, M. Khachani, A. Shaim, M. Boudalia, A. Sabbar, A. Ghanimi, A. Guenbour, A. Bellaouchou, Mater. Today Proc. **22**, 108 (2020)

28. A. Moguš-Milanković, A. Šantić, V. Ličina, D.E. Day, J. Non- Cryst. Solids **351**, 3235 (2005)
29. M. Laourayed, T. Guedira, A. Rhandour, Ann. Chim.- Sci. Mat. **23**, 319 (1998)
30. L. Baia, R. Stefan, W. Kiefer, J. Popp, S. Simon, J. Non-Cryst. Solids **303**, 379 (2002)
31. M. Abid, A. Shaim, M. Et-tabirou, Mater. Res. Bull. **36**, 2453 (2001)
32. R.K. Brow, D.R. Tallant, S.T. Myers, C.C. Phifer, J. Non-Cryst. Solids **191**, 45 (1995)
33. L. Montagne, G. Palavit, G. Mairesse, Phys. Chem. Glasses **37**, 206 (1996)
34. R.F. Bartholomew, J. Non- Cryst. Solids **7**, 221 (1972)
35. D.E.C. Corbrjdge, J. Appl. Chem. **6**, 456 (1956)
36. C. Garrigou-Lagrange, M. Ouchetto, B. Elouadi, Can. J. Chem. **63**, 1436 (1985)
37. H.S. Liu, T. Chin, S. Yung, Mater. Chem. Phys. **50**, 1 (1997)
38. M.A. Salim, G.D. Khattak, M.S. Hussain, J. Non- Cryst. Solids **185**, 101 (1995)
39. A.A. Kharlamov, R.M. Almeida, J. Heo, J. Non- Cryst. Solids **202**, 233 (1996)
40. L. Baia, T. Iliescu, S. Simon, W. Kiefer, J. Mol. Struct. **599**, 9 (2001)
41. A. Chahine, M. Et-tabirou, M. Elbenaissi, M. Haddad, J.L. Pascal, Mater. Chem. Phys. **84**, 341 (2004)
42. K. Majhi, K.B.R. Varma, Int. J. Appl. Ceram. Technol. **7**, E89 (2010)
43. A.A. Ali and M.H. Shaaban, Bull. Mater. Sci. **34**, 491 (2011)
44. V. Ravi Kumar, N. Veeraiah, J. Phys. Chem. Solids **59**, 91 (1998)
45. D.K. Durga, N. Veeraiah, J. Mater. Sci. **36**, 5625 (2001)
46. M. Peng, C. Zollfrank, L. Wondraczek, J. Phys.: Condens. Matter **21**, 285106 (2009)
47. N.F. Mott, E.A. Davis, Electronic processes in non-crystalline materials (Oxford University Press 2012)
48. Y.H. Na, N.J. Kim, S.H. Im, J.M. Cha, B.K. Ryu, J. Ceram. Soc. Jpn. **117**, 1273 (2009)
49. I. Boukhris, I. Kebaili, M.S. Al-Buriahi, B. Tonguc, M.M. AlShammari, M.I. Sayyed, Ceram. Int. **46**, 22883 (2020)
50. P.S. Rao, C. Rajyasree, A.R. Babu, P.M.V. Teja, D.K. Rao, J. Non- Cryst. Solids **357**, 3585 (2011)
51. J.E. Shelby, Introduction to glass science and technology (Royal Society of Chemistry, 2020)
52. J.A. Duffy, Phys. Chem. Glasses **42**, 151 (2001)

Cite this article as: Mohamed Laourayed, Yasmina Alaoui, Asmae Er-rafai, Mouad El Mouzahim, Mouloud El Moudane, Mohammed Abid, Mestapha Beraich, Abdellah Guenbour, Abdelkbir Bellaouchou, Structural, dielectric and optical properties of Ta_2O_5-Bi_2O_3-P_2O_5 phosphate glasses, Eur. Phys. J. Appl. Phys. **97**, 49 (2022)